Slow-growing reef corals as climate archives: A case study of the Middle Eocene Climatic Optimum 40 Ma ago

Thomas Brachert, Thomas Felis, Cyril Gagnaison, Marlene Hoehle, Markus Reuter, Philipp Spreter

GEOCHEMISTRY

Slow-growing reef corals as climate archives: A case study of the Middle Eocene Climatic Optimum 40 Ma ago

Thomas C. Brachert[1]*, Thomas Felis[2], Cyril Gagnaison[3], Marlene Hoehle[1], Markus Reuter[4], Philipp M. Spreter[1]

The skeletons of stony corals on tropical shallow-water reefs are high-resolution climate archives. However, their systematic use for unlocking climate dynamics of the geologic past is limited by the susceptibility of the porous aragonite skeleton to diagenetic alterations. Here, we present oxygen and carbon isotope time series (monthly resolution) from reef corals with an unusual unaltered preservation from the Middle Eocene Climatic Optimum (MECO) "hyperthermal" (40 million years ago). Annual extension of the corals at the studied midlatitude site (France) was remarkably low (0.2 cm). Nonetheless, isotope signatures display no evidence for kinetic disequilibria that discredit their use as climate archive, but growth rate–dependent annual signal amplitude attenuations need corrections using an innovative sampling approach. Thereafter, we present evidence of symbiotic zooxanthellae in reef corals of the Paleogene and subdued sea surface temperature seasonality of only 7° to 8°C during the MECO, consistent with the globally equant climate of the hothouse.

INTRODUCTION

The skeletons of stony corals (Scleractinia) of tropical shallow-water reefs represent excellent climate archives. As a result of high water temperatures [sea surface temperatures (SSTs)] over the entire year, the hemispherical, "massive," calcareous skeletons of the widespread genera *Porites* (Indo-Pacific) or *Orbicella* (Atlantic) exhibit high vertical growth rates (extension rates) of 1 cm year^{-1} and more. This allows for the generation of time series of proxy data for SSTs and many other environmental parameters with high, i.e., monthly to weekly, temporal resolution. Depending on the life span of the corals, these time series can cover periods of several hundreds of years and allow for an accurate description of past environmental change for regions without long, systematic weather records or from the deep geological past (*1*, *2*). As a result of seasonal temperature changes, the skeletons show a pronounced annual banding, which is imaged in x-radiographs as a sequence of alternating bands of high and low density (*3*–*5*). One high-low density band couplet typically represents 1 year of growth where the high-density portion of the couplets is usually formed during winter; however, variations exist between species and colonies (*3*, *6*). In combination with cyclic changes of skeletal bulk density, proxy data of SST records, such as oxygen isotope ratios ($\delta^{18}O$) or concentrations of certain trace elements (Sr/Ca and Li/Mg), provide the backbone for the construction of detailed internal chronologies (*2*). However, toward the limits of the latitudinal range of tropical shallow-water corals, as a result of decreasing SST and light intensity, extension rates decrease to a few millimeters per year or less, and growth pauses sometimes occur when winter SSTs fall below a critical threshold (*7*). For instance, the growth of *Porites* seems to slow down markedly or even stop below 18°C (*4*, *8*). As a result of slowed or halted growth during the cool season, time series of proxies commonly have a particularly low resolution during the cool season, and the corresponding proxy time series, e.g., of $\delta^{18}O$, and density patterns will show no more symmetrical sinusoids but rather an alternation of broad and rounded minima separated by narrower, more or less acute peaks representing the warm/cool growth season (*9*). Such cuspate patterns in growth and proxy data characterize skeletal growth at environmental limits (*10*). Taxa other than *Porites*, however, such as the tropical to warm temperate *Plesiastrea*, display continuous skeletal accretion over the entire year, even within marginal positions of the reef belt at high latitudes where winter SSTs are as low as 10°C and light intensity is up to 70% lower than in the tropics (*6*, *7*, *11*). Within such marginal growth environments, where SSTs range seasonally between 10° and 25°C, annual extension rates of *Plesiastrea* drop to a minimum of 0.1 cm (*6*, *11*). However, despite continuous growth at low SSTs and over periods of several hundred years, the potential of these massive reef corals as climate archives of the subtropical and warm temperate zones is little studied (*6*), and no SST proxy records exist to date. This is unexpected with regard to the potential role of the subtropical and warm temperate zones as future refugia for tropical reef corals in a warming ocean or because of potential increases in bleaching risks even at these high latitudes (*12*, *13*).

Beyond technical problems of sampling resolution and sample powder quantity, however, the use of stable isotope proxy data from these corals is complicated by a number of effects arising from low extension rates: (i) Sampling bias—reconstructed signal amplitude primarily depends on sampling resolution (*14*). However, at small extension rates, resolution is limited by critical sampling volumes, and reconstructions will therefore underestimate true seasonality. (ii) Stable isotope effects—corals precipitate a rigid skeleton of aragonite ($CaCO_3$) that is depleted in ^{18}O relative to ambient seawater (*15*). However, this depletion of ^{18}O is not constant. For example, it is subject to the so-called vital effects in fast-growing massive corals, which allow an application as a (paleo-)thermometer. However, for these applications, the ratio of ^{18}O and ^{16}O (expressed as $\delta^{18}O$ value) in seawater must be known or, in case of subannual reconstructions, can be assumed to be constant over the year (*2*). Complications of

[1]Institute for Geophysics and Geology, University of Leipzig, Talstrasse 35, 04103 Leipzig, Germany. [2]MARUM—Center for Marine Environmental Sciences, University of Bremen, Leobener Str. 8, 28359 Bremen, Germany. [3]Département de Géosciences, B2R-EA 7511, UniLaSalle, Terre & Sciences (Site de Beauvais), 19 Rue Pierre Waguet, BP30313, F-60026 Beauvais CEDEX, France. [4]Institute of Geography and Geology, University of Greifswald, Friedrich-Ludwig-Jahn-Strasse 17a, 17489 Greifswald, Germany.
*Corresponding author. Email: brachert@uni-leipzig.de

the $\delta^{18}O$ thermometer exist, however, because the offset of $\delta^{18}O$ values between coral and seawater can vary substantially between single skeletons from one site with homogeneous SST structure ("intercolony offsets") (*16*). At constant SSTs, mean (annual or colony) $\delta^{18}O$ values of coral aragonite were also shown to be dependent on extension rate, if growth declines below 0.4 to 0.6 cm $year^{-1}$, a pattern that has been explained by extension rate–related kinetic isotope disequilibrium effects (*16*–*19*). (iii) Biosmoothing—the thickness of the tissue layer varies among reef corals, even in one single genus, thereby influencing the duration of skeletal thickening relative to vertical growth. This process of "biosmoothing" causes individual expressions of time averaging in proxy records among corals (*20*). Attenuation of subannual signal variability by biosmoothing becomes increasingly prominent at low vertical extension rates of the skeletons, because the skeleton remains in contact with the precipitating tissue for a prolonged period of time (*20*). For that reason, $\delta^{18}O$-SST sensitivity of corals on sub- to interannual time scales is always less than the established value of −0.23 per mil (‰)/°C for biogenic and inorganic aragonite and requires specific, extension rate–dependent calibrations (*20*). Furthermore, the calibration slope will necessarily differ between intra-annual and annual or mean coral data (*20*, *21*). Thus, in instances where seasonality and long-term changes are to be inferred from fossil corals and no a priori knowledge of the style of biosmoothing is available, the study of relatively fast-grown corals that likely underwent little smoothing was recommended (*16*, *20*). A more comprehensive account on the problem of biosmoothing and sampling procedures involved in geochemical analyses of reef corals was given by Sadler *et al.* (*22*).

Here, we present records of subannually (monthly) resolved proxy data ($\delta^{18}O$ and $\delta^{13}C$) of massive reef corals (*Astreopora*) with ultralow extension rates. Our study is peculiar because the corals investigated deriving from the Middle Eocene Climatic Optimum (MECO) ~40 million years (Ma) ago are the oldest coral records published so far, and the paleolatitude of growth of ~45°N represents one of the northernmost occurrences of shallow-water reef corals during the entire Cenozoic (66 to 0 Ma). For this work, we use a fine-scale approach of powder milling for mass spectrometry (*23*) and test published correction methods for growth rate–related isotope effects and biosmoothing on the $\delta^{18}O$ data from slow-growing corals. For establishing a correction method for coral $\delta^{18}O$ seasonality at exceptionally small extension rates, we generated monthly resolved $\delta^{18}O$ records along diverging growth axes (corallites) of one single coral specimen (corallum) that document spatially heterogeneous extension rates between 0.1 and 1.4 cm $year^{-1}$ within common years. Results with a replication specimen demonstrate that reef corals with ultralow extension rate from subtropical and temperate regions are highly valuable environmental archives, even at ultrahigh subannual resolution, if corrections can be made. The purpose of this paper is (i) to present a way to prepare an empirical calibration for $\delta^{18}O$ seasonality if no instrumental SST data are available and the underlying processes of isotope fractionation and biosmoothing are unknown, and (ii) to demonstrate zooxanthellate symbiosis in tropical reef corals of the Paleogene (66 to 23 Ma).

The middle Eocene case study

Climate

The Early Paleogene "hothouse" (56 to 47 Ma) was the warmest geological period of the Cenozoic (*24*). In the course of the Eocene (56 to 34 Ma), equatorial SSTs declined by ~5°C, reaching approximately modern values during the late Eocene, while the mid and high latitudes remained 10° to 20°C warmer than at present (*25*, *26*). Superimposed on the long-term cooling trend were short transient warmings ("hyperthermals"), the last of which was the MECO that occurred during the Bartonian, ~40 Ma ago (*27*, *28*). With regard to other hyperthermals, the MECO was peculiar because of its long duration (0.4 Ma) effected by CO_2 from a flare-up of continental arc volcanism (*29*, *30*) and a delayed drawdown of atmospheric CO_2 (*30*). As result of the atmospheric pCO_2 rise, global ocean temperatures increased by 2° to 5°C, and surface waters acidified by up to ~0.2 pH units above middle Eocene background values (*28*, *31*, *32*).

For the middle Eocene (48 to 38 Ma), marine and terrestrial proxy data document a globally warm and rather humid climate with above-freezing extratropical temperatures (*25*, *28*, *33*, *34*). Although modeling middle Eocene climate still holds many challenges, at realistic levels of atmospheric greenhouse gases, models reproduce the global picture derived from proxy data fairly well (*26*, *33*, *35*). Long-term trends in seasonality of air temperatures based on terrestrial plant associations not only demonstrate attenuated seasonality for Atlantic and Pacific coastal regions of Eurasia and on Greenland but also reveal that long-term Eocene cooling essentially reflects a decrease in winter temperatures while summer temperatures remained constant (*33*, *34*, *36*). A global trend of long-term seasonality increase can now be well explained in models by the combined effect of CO_2 decrease, falling sea level, and formation of sea ice around 38 Ma (*33*, *37*). However, the methodology of the coexistence approach applied for terrestrial reconstructions is based on the climatic tolerances of all nearest living relatives within a fossil flora (*38*) and therefore strongly depends on assumptions, but in no case can this methodology provide continuous time series of seasonal variations (*38*). Subannually resolved $\delta^{18}O$ time series of SST seasonality are available only through molluscan sclerochronologies from Western Europe and the U.S. Gulf region area that mostly demonstrate low seasonal contrasts for the middle Eocene (*10*, *39*–*49*). However, the significance of these sclerochronologies is severely biased by taxonomical diversity and habitat heterogeneity (shallow versus deep, epi- versus endobenthic, oligo- versus eutrophic, etc.) of the taxa studied, but, most importantly, by nearshore hydrologic effects on isotopic signatures (freshwater discharge and precipitation/evaporation), rhythmic growth interruptions, and resolution artifacts, to name a few (*10*, *49*). While there is no evidence from these data for a long-term change in seasonality, an increase in seasonality from the middle Eocene to the Oligocene is inferred from sclerochronologies of fish otoliths of the U.S. Gulf Coast region (*39*). In this respect, however, despite all uncertainties, the sclerochronologies certainly fit into the concept of a reduced seasonality within the context of an equant Eocene climate (*35*).

Shallow marine benthic communities in Northwestern Europe

In continental northwestern (NW) Europe, located during the middle Eocene at ~45°N latitude (*50*), paratropical terrestrial vegetation (e.g., palms) and vertebrate fauna (*Trionyx*, *Diplocynodon*, *Lophiodon*, *Propalaeotherium*, and *Hyaenodon*) prevailed (*34*, *51*). Along the Atlantic coast, a shallow gulf spanned much of southern England, the English Channel, and northern France [Paris and Hampshire basins (PB-HB)], housing a highly diverse tropical benthic community (Fig. 1). In PB, marine mollusk diversity peaked during the Lutetian-Bartonian (>2500 species) (*51*). The mollusks, foraminifers, and dasycladacean calcareous algae hint to the presence of very

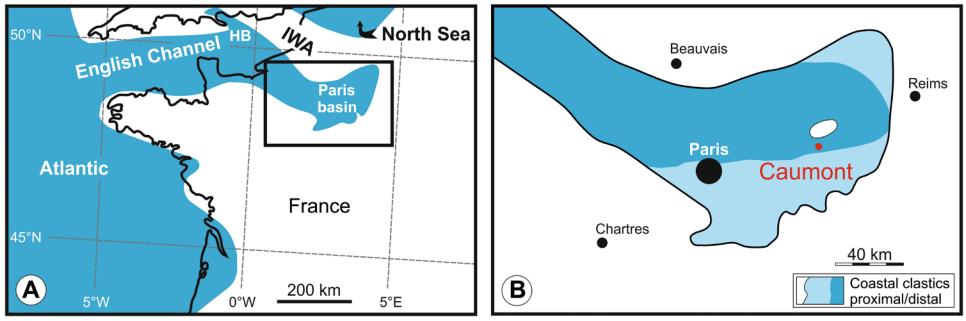

Fig. 1. Paleogeography of NW France (PB) during the middle Eocene (Bartonian). (**A**) A marine gateway connecting the northeast Atlantic to the North Sea was closed by the late Lutetian through uplift of the Isthmus of Weald-Artois (IWA), preventing any further influx of cool and brackish waters from the Arctic and North Sea (*26*) into the PB-HB. The black rectangle shows the position of (B). (**B**) Marine facies distributions during the Bartonian (Sables d'Auvers); from (*54*), modified. The sampling site (Caumont) was in a rather protected position of the shallow gulf. Black contours in (A) represent the present-day coastlines; the grid shows modern coordinates.

shallow subtidal and oligotrophic environments with seagrass vegetation (*52*, *53*). Reef corals occurred during three rather short episodes of the middle and late Lutetian as well as the Bartonian (MECO) (*51*, *53*, *54*), forming the northernmost occurrences of the entire Cenozoic (*55*, *56*). Although true framework reefs seem not to have existed within the gulf, the diversity of reef corals with hemispherical and pillow-like growth forms (massive) alike *Astreopora*, *Goniopora*, and *Porites* together with branching *Acropora* was rather high (≥9 genera) (Fig. 1) (*55*, *57*). Mean annual SSTs inferred from reef coral diversity were ~19°C (*55*). Reconstructions of Bartonian SSTs based on clumped isotope thermometry tend to be higher but are only available for the open ocean at higher and lower latitudes, respectively, and are therefore not directly comparable (*25*).

Eocene fossils of PB have since the 19th century been well known for their excellent preservation. In contrast to other marine deposits of this age, skeletal aragonite of mollusks and reef corals is fully preserved with all original detail and porosity, sometimes even with original coloration (*51*, *55*). Because of the excellent preservation of aragonite fossils, stable isotope data from branching *Acropora*, mollusks (bivalves and gastropods), and calcareous algae from PB and HB have been presented (*44*, *46*–*48*, *55*). Reef coral specimens investigated during this study were collected near Caumont (PB), from the mostly unlithified sands of the Sables d'Auvers unit, and are Bartonian (~40 Ma), equivalent with the MECO (Fig. 1) (*54*).

RESULTS

Two specimens of the coral genus *Astreopora* were selected for this study according to their growth patterns and preservation (Materials and Methods). Both specimens show more or less flat to slightly convex, narrow annual growth bands in three-dimensional (3D) space, crossed by parallel, vertically arranged corallites (Fig. 2 and fig. S1). In specimen CAU-A3, the density banding documents vertical extension rates between 0.3 and 0.4 cm year^{-1} (Table 1). The same principal pattern holds for specimen CAU-D4. As a major difference, however, in the upper third of the fragment, the vertically arranged corallites terminate along an irregular erosion surface that is more or less flat in 3D and essentially parallel to the growth bands. Overgrowth along the erosion surface is by corallites orientated parallel to the discontinuity in their initial stages and turning upward and vertical in their late stages of growth. In the early stage of growth, which is parallel to the erosion surface and was originally horizontal, extension rate was rapid ≤1.4 cm year^{-1} and declined toward ~0.2 cm year^{-1} in the late stages of growth of the corallites (Table 1). Although the corallite arrangement resembles that of columnar coral colonies showing rapid vertical growth in the center of the column and slow horizontal growth in peripheral zones in 2D x-radiographs, the arrangement of corallites reflecting rapid horizontal/slow vertical growth in specimen CAU-D4 is due to a growth anomaly along a rather flat, originally more or less horizontal surface in 3D. This anomalous growth pattern represents a well-known strategy of encrusting reef corals to rapidly occupy empty hard spaces and massive reef coral colonies to ensure quick reoccupation of free hard surfaces that were given up by the colony previously because of diseases, bleaching, siltation, etc. (fig. S5) (*58*, *59*). The presence of bivalve borings penetrating the corallum from the discontinuity downward shows that it took some time for the discontinuity to be overgrown; according to the density banding, complete overgrowth took more than 5 years (Fig. 2D). Here, we use the pattern for a comparative analysis of isotope variability as a function of extension rate, comparable with previous studies on modern corals but differing by the spatial orientation of the corallites with rapid/slow growth (*17*). The positioning of the sampling transects covers a total period of 4 years for comparative analysis (Fig. 2).

Specimen CAU-A3

$\delta^{13}C$ values range from −5.02 to −1.52‰ Vienna Pee Dee Belemnite (VPDB) (mean: −2.92 ± 0.88‰ VPDB), $\delta^{18}O$ values range from −7.11 to −5.61‰ VPDB (mean: −6.41 ± 0.36‰ VPDB), and a significant negative correlation exists between $\delta^{18}O$ and $\delta^{13}C$ (Fig. 3). $\delta^{18}O$ shows cycles in accordance with the density banding; most positive values of $\delta^{18}O$ representing the cool season coincide with bands of maximum bulk density, and most negative values representing the warm season coincide with minima of bulk density (Fig. 4A). This relationship is in full accordance with the patterns of many modern reef corals (*3*, *5*, *60*) and allows reading the Eocene record with criteria relevant to modern corals. Clearly, no diagenetic alteration has taken place in an extent sufficient to alter the excellent fit of the paired density and isotope signatures, even if localized diagenetic alterations are microscopically recognizable. We therefore attribute the sometimes comparatively high calcite concentration (≤3% according to x-ray diffraction) to contaminations by sediment

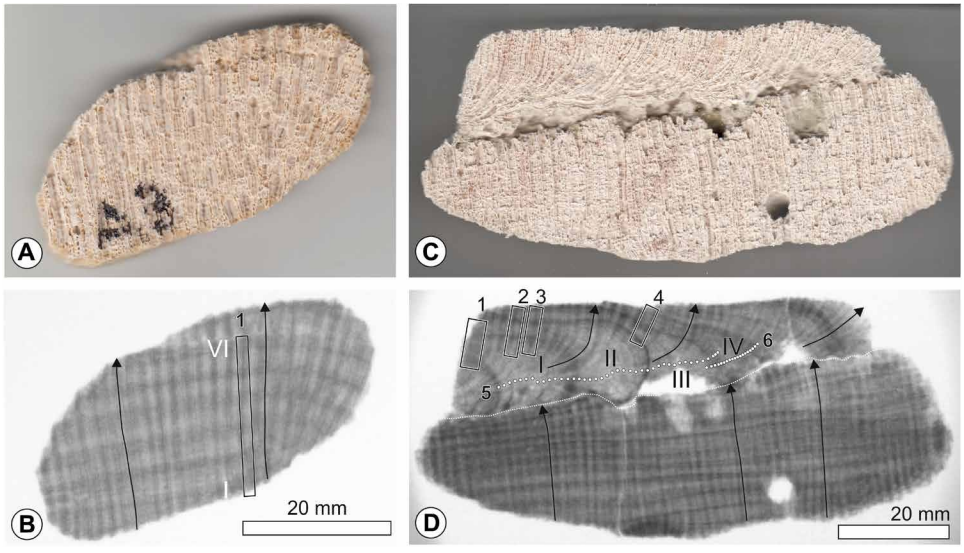

Fig. 2. Photographs of slabs of two specimens of *Astreopora* and their corresponding x-ray images (positive prints). Slabs were cut parallel to the plane of corallite growth. The x-radiographs show distinct annual density bands. In the radiographs, black arrows follow the growth trajectories of single corallites; Latin numbering refers to years of the internal chronologies. (**A** and **B**) CAU-A3: Black rectangle delineates sampling transect 1 for years I to VI. Year #VII broke off during preparation of the ledge along a band of very low density and was lost for further analysis. (**C** and **D**) CAU-D4: Numbered black boxes delineate the position of ledges cut out of the slab for milling of consecutive isotope samples (#1 to #4). Transects #5 and #6 were sampled by drilling (white dots). Transects #2 and #3 were also used for a replication test of the stable isotope patterns (fig. S4). The thin, white stippled line marks a growth discontinuity (and limit between a lower/upper subsample CAU-D4u and CAU-D4o); specimen CAU-D4 may originally represent coralla from two separate colonies. Photo credit: T. C. Brachert/P. M. Spreter, Leipzig University, Germany.

Table 1. Data summary, specimens CAU-A3 and CAU-D4, and SST reconstructions according to a mean coral calibration (−0.22‰ change in $\delta^{18}O$/°C) (*61*).

Coral specimen	Transect #	Year #	Annual extension (cm)	Number of samples per year	Annual $\delta^{13}C$ (‰ VPDB)	Seasonal $\delta^{13}C$ contrast (‰ VPDB)	Annual $\delta^{18}O$ (‰ VPDB)	Seasonal $\delta^{18}O$ contrast (‰ VPDB)	Seasonal SST contrast (°C)	Seasonal SST contrast (°C) corrected
CAU-A3	T1	1	0.40	18	−2.60	2.10	−6.38	0.94	4.3	6.6
CAU-A3	T1	2	0.39	19	−2.69	2.34	−6.58	1.06	4.8	7.2
CAU-A3	T1	3	0.41	26	−3.00	2.60	−6.42	1.14	5.2	7.5
CAU-A3	T1	4	0.31	16	−3.11	2.39	−6.30	1.10	5.0	8.1
CAU-A3	T1	5	0.36	14	−3.07	2.78	−6.39	1.31	6.0	8.6
CAU-D4o	T1	1	0.47	24	−3.17	2.57	−6.72	1.36	6.2	8.0
CAU-D4o	T2	2	0.27	22	−2.58	2.52	−6.44	0.73	3.3	6.8
CAU-D4o	T2	3	0.17	9	−2.45	2.03	−6.55	0.62	2.8	7.7
CAU-D4o	T3	2	0.27	17	−2.72	2.35	−6.45	0.69	3.1	6.6
CAU-D4o	T4	3	0.22	13	−2.82	2.08	−6.76	0.55	2.5	6.6
CAU-D4o	T4	4	0.17	14	−2.80	2.18	−6.57	0.63	2.9	7.7
CAU-D4o	T5	1	1.39	13	−3.21	1.97	−6.61	1.69	7.7	7.8
CAU-D4o	T5	2	1.34	12	−3.46	2.02	−6.52	1.36	6.3	6.2
CAU-D4o	T5	3	1.16	12	−2.84	1.89	−6.69	1.60	7.3	6.2
CAU-D4o	T6	4	0.66	16	−2.48	2.48	−6.81	1.40	6.3	7.3

particles that were removed in an ultrasonic bath before stable isotope analysis (fig. S3). Diagenetic alterations of the skeleton, although present, are therefore irrelevant in extent for substantially altering stable isotope signatures. Nonetheless, our better than monthly resolution $\delta^{18}O$ data indicate mean SST seasonality of only 5.1° ± 0.6°C when assuming a typical temperature sensitivity for reef corals of −0.22‰ change per 1°C and a constant intra-annual $\delta^{18}O$ value of ambient seawater (Table 1) (*61*). When read as a guide to the symbiotic/asymbiotic mode of life of the coral colonies, mean $\delta^{13}C$ values indicate that the Eocene *Astreopora* were, like their

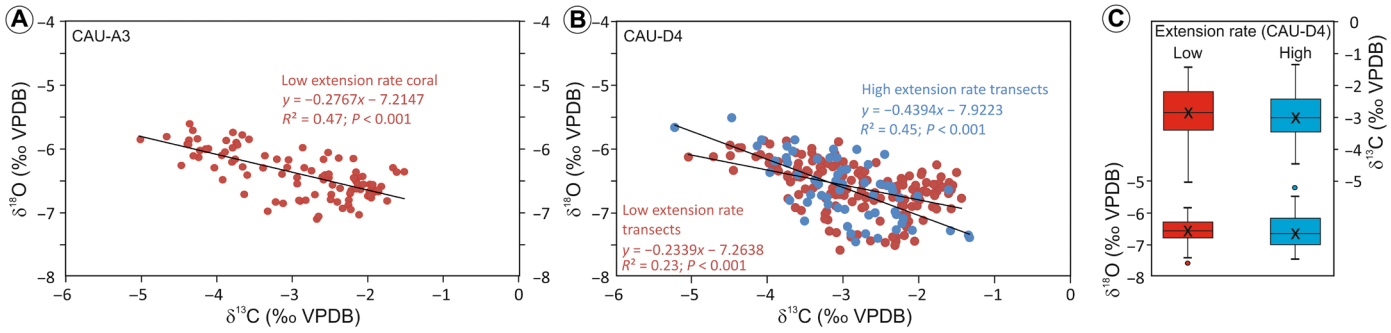

Fig. 3. Stable isotope systematics of Eocene *Astreopora*. (**A** and **B**) Cross-plots of $\delta^{13}C$ and $\delta^{18}O$ values for specimens CAU-A3 ($n = 102$) and CAU-A4 ($n = 225$), respectively. (**C**) Box plots of $\delta^{13}C$ and $\delta^{18}O$ values from slow-grown (0.1 to 0.4 cm year^{-1}, red) and fast-grown (0.4 to 1.4 cm year^{-1}, blue) corallites show that there is no difference in the mean values between these corallites (specimen CAU-D4). Means of $\delta^{18}O$ and $\delta^{13}C$ values from transects with low and high extension rate are indistinguishable according to a *t* test for $\alpha = 0.05$.

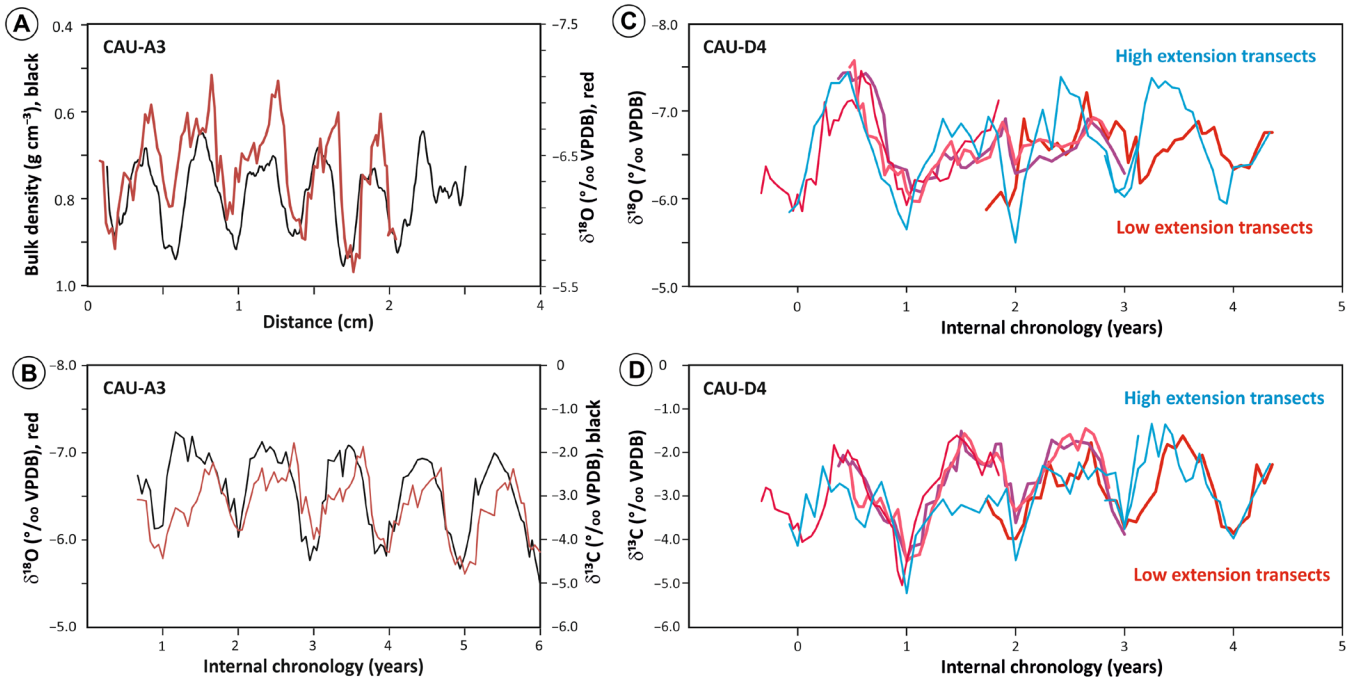

Fig. 4. Time series of $\delta^{13}C$ and $\delta^{18}O$ values (raw data, no smoothing). Note that the vertical scales for bulk density and $\delta^{18}O$ values have been inverted to highlight the underlying temperature effect. (**A**) Oxygen isotope ratios ($\delta^{18}O$ values) and bulk density plotted against sampling distance to show excellent fit of stable isotope cycles with density banding at submillimeter scales (CAU-A3). (**B**) Time series of $\delta^{18}O$ and $\delta^{13}C$ values (CAU-A3). (**C** and **D**) Time series of $\delta^{18}O$ and $\delta^{13}C$ values from corallites with high (blue) and low extension rates (red), respectively. Note the distinct interannual trends of both records (CAU-D4).

modern relatives, zooxanthellate (fig. S7) (*62*). The cyclic patterns further imply that a maximum of symbiont photosynthesis occurred during summer, in agreement with present-day weather systems and seasonal irradiance patterns at a paleolatitude of ~45°N (*50*, *63*, *64*). Because there is no conspicuous phase shift between the $\delta^{18}O$ and $\delta^{13}C$ cycles, the coolest/warmest SSTs were likely reached coeval with the shortest/longest day in a year.

Specimen CAU-D4

$\delta^{13}C$ values range from −5.23 to −1.34‰ VPDB (mean: −2.89 ± 0.77‰ VPDB), $\delta^{18}O$ values range from −7.58 to −5.51‰ VPDB (mean: −6.60 ± 0.41‰ VPDB), and a significant negative correlation exists between $\delta^{18}O$ and $\delta^{13}C$ (Fig. 3). The cycles of $\delta^{18}O$ and $\delta^{13}C$ are fully consistent with the density bands, both in transects with high and low extension rate, and are comparable to the pattern and relationship observed in specimen CAU-A3 (Figs. 2D and 4A). To identify growth rate effects in our $\delta^{18}O$ records from *Astreopora*, we use a special arrangement of sampling transects that allow comparing reconstructions of seasonality from records of the same years but showing differencing extension rates between 0.2 and 1.4 cm year^{-1} depending on the orientation of the transects (Fig. 2D and Table 1). All transects were sampled as to reach a mean monthly resolution

(≥12 samples year^{-1}). For the individual transects and years, we found very heterogeneous seasonal SST contrasts; the transect with the highest extension rate (#5) shows the highest mean seasonal range of $\delta^{18}O$ values, equivalent with 7.1°C using the same assumptions as for specimen CAU-A3 (Table 1). This reconstruction being substantially higher than for specimen CAU-A3 is still below the present-day seasonality at equivalent latitudes off western France and within sheltered embayments (10° to 15°C; fig. S6), but consistent with an attenuated seasonal contrast because of a globally equable climate during the Eocene (*35*). Table 1 lists all transect details on sampling resolution, extension rate, mean annual $\delta^{18}O$ and $\delta^{13}C$, and mean seasonal ranges of $\delta^{18}O$ and $\delta^{13}C$ values.

DISCUSSION

The parallel, slightly convex upward density bands of the two corals are the expression of a pillow-shaped or hemispherical growth form of the coral colonies. In the upper third of specimen CAU-D4, a growth anomaly causes the extension rate to be large in transects along horizontal corallites, but small in transects along oblique- or vertical-oriented corallites, which is actually unusual for massive pillow-shaped corals, but in the case of CAU-D4, it is either the result of a lesion or the reflection of an encrusting growth form that documents at early growth stages rapid occupation of growth surfaces available (Fig. 2 and fig. S5) (*58*, *59*). Differencing signal amplitudes were observed along the transects for each year, with large amplitudes of $\delta^{18}O$ values for high extension rates along horizontal transects (#5 and #6) and small amplitudes for small extension rates on oblique to vertical transects (#1 to #4) (Table 1). In this way, any given year within our time series of 4 years' duration can show very different amplitudes of $\delta^{18}O$ values depending on the extension rate that varies with the orientation of a transect (Table 1). We tested three hypotheses as explanations for this phenomenon: (i) sampling bias—signal amplitude is controlled by sampling density because transects with small extension rates accommodate less samples along spatial transects (lower spatial resolution), thereby documenting an attenuated amplitude (*14*). However, all transects were sampled at a spatially different but temporally uniform, quasi-monthly resolution based on the radiograph, regardless of the extension rate. Accordingly, differences in signal amplitude between transects and within transects are not due to a sampling bias. However, we cannot quantify the possibility that the cool season is underrepresented within a year as a result of lower extension than in the warm season; a weak cuspate pattern of the $\delta^{18}O$ and $\delta^{13}C$ cycles suggests that this is the case (Fig. 4) (*10*). Nonetheless, a distinct V-shaped pattern representing the cool season is not present in bulk density and the isotope cycles that rather document continuously slow but not halted growth. (ii) Stable isotope kinetics—available data suggest that kinetic isotope effects more or less completely override the vital effect if annual extension rates fall below 0.4 or 0.6 cm and drive both isotope systems (annual and multiyear averages) to increasingly positive values as a consequence of a trend toward equilibrium fractionation. This trend results in a pronounced, positive correlation of the $\delta^{18}O$ and $\delta^{13}C$ values (*16*, *17*, *65*). However, these predictions are not borne out by our measurements. Rather, the spread of the data is low, annual mean values of $\delta^{18}O$ and $\delta^{13}C$ show no correlation ($P = 0.6$), and a trend toward more positive mean values at low extension rates is not present between extension rates of 0.2 and 1.4 cm year^{-1} in either isotopic system ($\delta^{13}C$: $P = 0.3$; $\delta^{18}O$: $P = 0.7$) (Figs. 3 and 5). For this reason, we can exclude a relevant kinetic effect on $\delta^{18}O$ and $\delta^{13}C$ values for the extension rates we investigated, so that a use as proxy data is possible without any sort of correction. In addition, so-called intercolony offsets (*16*, *65*) should not play a role under these circumstances and are not indicated from the data documented by the replication specimen (Fig. 3). Our finding supports earlier suggestions that conceptual models based on just inorganic carbonate chemistry are likely too simplistic to explain skeletal stable isotope variability in reef corals (*66*). A mechanistic interpretation of this result is, however, beyond the scope of this fossil analog study. Rather, the focus of our work is to document the suitability of these slow-growing, massive corals as environmental archive. (iii) Biosmoothing has two severe implications for environmental proxy data: First, at extension rates <0.6 cm year^{-1}, proxy data from massive *Porites* have a substantially attenuated seasonal signal amplitude relative to a forcing, and second, the degree of signal attenuation is modulated by the efficient tissue thickness of a given colony (*20*). In contrast to constant annual mean values, a tendency for a significantly reduced seasonal contrast in $\delta^{18}O$ values does exist below an extension rate of 1.0 cm year^{-1} (Table 1). This relationship replicates an earlier observation by an interspecies comparative study, that is, attenuations of seasonal proxy amplitudes are not relevant at extension rates >0.45 cm year^{-1} (*20*, *65*). In our fossil data, the change in signal amplitude at extension rates <1.0 cm year^{-1} apparently occurs because of a simultaneous change in winter and summer values toward the annual mean, rather than toward increasingly positive values, as would be expected from kinetic isotope effects (Figs. 3 and 4). In

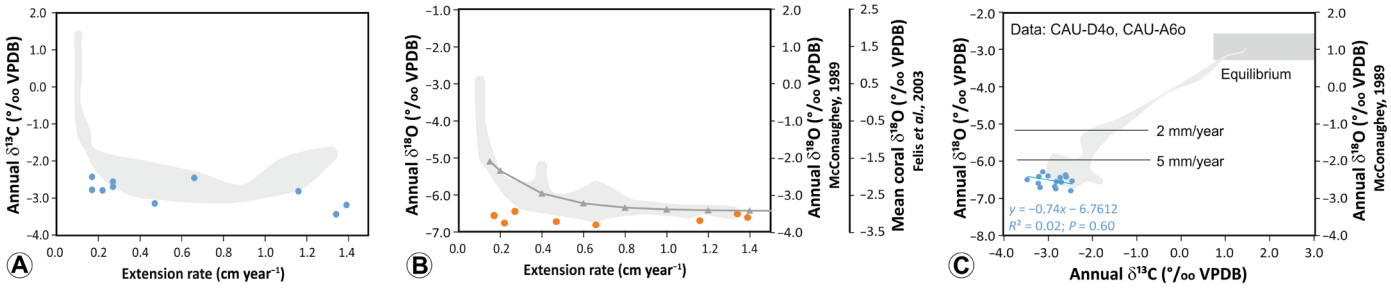

Fig. 5. Relationship of annual values of $\delta^{13}C$ and $\delta^{18}O$ with annual extension rate. (**A**) Annual $\delta^{13}C$ values plotted against annual extension rate; gray shade delimits McConaughey's 1989 data (identical scales) (CAU-D4). (**B**) Annual $\delta^{18}O$ values plotted against annual extension rate; gray shade shows McConaughey's 1989, and gray triangles show the result of a replication study on mean coral data (CAU-D4) (*16*). (**C**) Cross-plot of annual $\delta^{13}C$ and $\delta^{18}O$ values; gray shades and extension limits represent McConaughey's 1989 data (*17*). Note the small spread of isotope data relative to McConaughey's data; all plots with coherent scaling.

this respect, the general prediction of the biosmoothing hypothesis is verified. However, this pattern only affects the amplitude of the $\delta^{18}O$ cycles, whereas the seasonal contrast of the $\delta^{13}C$ cycles is not attenuated between extension rates of 0.2 and 1.4 cm year^{-1}, i.e., constant at all extension rates studied (seasonal contrast of $\delta^{13}C$ = 2.21 ± 0.25‰) (Figs. 4 and 6, Table 1). In this respect, the $\delta^{13}C$ proxy conserves a primary environmental signal without evidence for attenuations of signal amplitude, in agreement with the already fairly large signal amplitude of the $\delta^{13}C$ cycles. Thus, signal attenuation at small extension rates selectively affects only oxygen isotope ratios. The absence of an extension rate effect on $\delta^{13}C$ has been noted earlier by a study on branching reef corals (*64*). In line with these findings, a previous study using aliquots from the same samples for stable isotope and trace element analyses showed that attenuation of $\delta^{18}O$ variability was related to extension rate, while that of the Sr/Ca proxy for SST was not (*67*). However, Sr/Ca and other trace elements considered SST sensitive in many studies (Mg/Ca and Li/Ca) were shown to be linked with extension rate or not systematically linked with temperature, respectively (*68*–*70*). In this respect, the individual proxies are affected differently by biosmoothing and other growth rate effects, and each requires specific correction factors, if any. For that reason, we consider biosmoothing unlikely an adequate mechanism to explain the observed signal attenuation restricted to the $\delta^{18}O$ system; however, the purely empirical approach taken here lacking any instrumental data is not suited for a mechanistic understanding of the patterns. For this reason, the term "biosmoothing" is used in a purely descriptive way for the observed trend of signal attenuation of $\delta^{18}O$ seasonality and referred to in quotation marks.

Potential as proxy archive

Our data show very clearly that no kinetic effects on $\delta^{18}O$ and $\delta^{13}C$ values need to be assumed for the corals studied and thus allow direct inferences to be made about interannual environmental dynamics at the site (annual mean values) or long-term global trends (colony mean values). For example, it is remarkable to note how similar the annual $\delta^{13}C$ values recorded from the Eocene are to those of present-day reef corals, while the annual $\delta^{18}O$ values are much more negative than those of present-day reef corals—to use McConnaughey's example (*17*), largely identical in $\delta^{13}C$ value but ~3‰ more negative in $\delta^{18}O$ (Fig. 5). Presumably, this reflects a roughly similar global seawater $\delta^{13}C$ value during the MECO and at present day, but a ~3‰ more negative $\delta^{18}O$ value during the latter, consistent with deep sea data (*24*).

The annual amplitude of the $\delta^{13}C$ cycle was, on average, 2.2 ± 0.3‰ (2.3 ± 0.2‰ for low extension rates and 2.1 ± 0.3‰ for rapid extension; CAU-D4) and 2.4 ± 0.3‰ (CAU-A3) in the two corals, respectively (Table 1). This seasonal contrast is high with respect to present-day's variability in most shallow-water reef corals. Although extreme annual $\delta^{13}C$ changes may represent the expression of complex local processes of organic matter cycling and/or external inputs and turbidity, high $\delta^{13}C$ seasonality may equally be the expression of an enhanced, annual light-driven productivity contrast of photosynthesis by the symbionts at ~45°N paleolatitude relative to reef corals being currently restricted to the tropical and subtropical latitudes (*63*, *71*, *72*).

Regarding the annual amplitude of $\delta^{18}O$ values, transects with high extension rates (#5 and #6) allow a rather realistic reconstruction of seasonality, here for 4 years. In contrast, for the transects with low extension rates (#1 to #4), a substantial attenuation of the seasonal amplitude exists (Fig. 6). To quantify the attenuation effect of the Eocene material at extension rates <1.0 cm year^{-1}, a von Bertalanffy fit (*73*) was used to describe the relationship between annual extension rate and amplitude of the $\delta^{18}O$ values according to Eq. 1

$$\delta^{18}O \text{ signal amplitude } [‰] = 1.5968 * (1.0 - 1.158 * \mathrm{EXP}(-3.2061 * \text{extension rate } [\text{cm year}^{-1}])) \quad (1)$$

The mean deviation (1 SD) of the data from the von Bertalanffy regression is ±0.13‰ $\delta^{18}O$. In this respect, the agreement with the data is very good; the saturation of the function (99%) is reached at an extension rate of 1.6 cm year^{-1} (seasonal contrast of $\delta^{18}O$ values at a saturation of 1.59‰). Correspondingly, the measured seasonal contrast is reduced by ≤5‰ at extension rates >1.0 cm year^{-1}, but by 40 to 80% for extension rates between 0.3 and 0.1 cm year^{-1} (Fig. 6). The fit of the replication specimen to the von Bertalanffy regression is ±0.17‰ $\delta^{18}O$ and thus within the same magnitude as

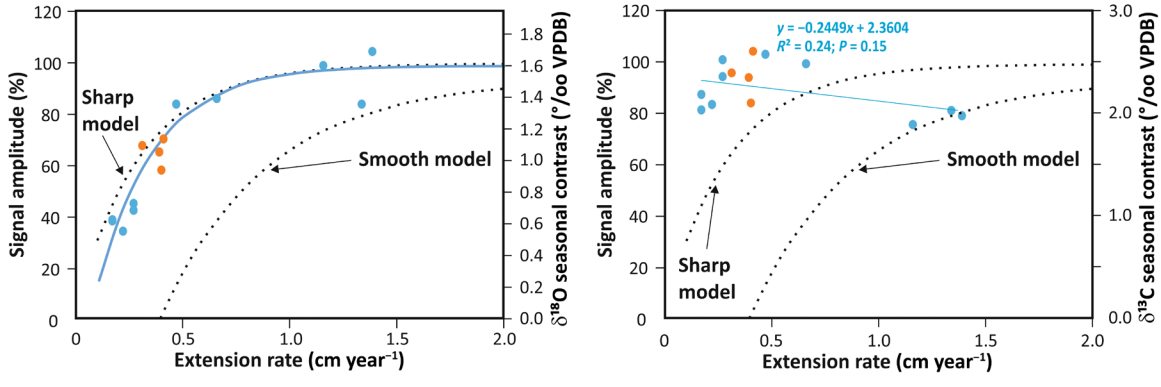

Fig. 6. Possible biosmoothing effect on recorded seasonal contrasts of $\delta^{13}C$ and $\delta^{18}O$ values for specimen CAU-D4 (blue dots). The blue line represents a von Bertalanffy fit to the data. The saturation value (1.59‰ of $\delta^{18}O$ seasonal contrast at 1.6 cm year^{-1}) was tuned to a signal amplitude of 100%. The data from the replication specimen (CAU-A3) are shown as orange dots (not part of the regressions). The sharp and smooth models of signal attenuation (*20*) and their extrapolation for extension rates <6 mm year^{-1} are also shown (stippled lines). Statistics for von Bertalanffy fit for 95% confidence interval of the general equation $y = a - (1 - be^{-cx})$ (*73*): a = 1.5968 (−21.47; 1.766); b = 1.158 (−0.4953; 1.467); c = 3.2061 (−0.2232; 6.375).

for the calibration. This finding allows a corrected estimate of mean SST seasonality of 7.1 ± 0.7°C (min: 6.2°C, max: 8.0°C; n = 10) for CAU-D4 and 7.6 ± 0.8°C (min: 6.6°C and max: 8.6°C; n = 5) for CAU-A3 for a change in $\delta^{18}O$ value of −0.22‰ change per degree Celsius as a widely accepted mean calibration for reef corals (Table 1) (*61*). The regression for our data is largely identical with the "sharp" model predictions for biosmoothing (*20*). Although this similarity seems to imply a similar net effect of proxy time averaging and efficient tissue thickness, we consider biosmoothing (*20*) as an unlikely mechanism for the observed signal attenuation, as it does not affect all proxies in the same way. Thus, given the possibility for overcoming extension rate effects on the amplitude of the $\delta^{18}O$ cycles, slow-grown reef coral skeletons represent rewarding archives of environmental dynamics on subannual time scales.

Constraints on middle Eocene paleoclimate scenarios

Our reconstruction of mean SST seasonality in the PB gulf ~40 Ma ago is based on continuous time series with a quasi-monthly resolution and cross-checked with independent internal chronologies based on the annual density bands of the corals. Furthermore, the replication experiment (CAU-A3) reveals that the attenuation effect on the seasonal $\delta^{18}O$ amplitude is consistent among coral specimens from the Caumont site and allows for a robust estimate of 7° to 8°C of seasonal SST contrast during the MECO using the calibration presented here. We note that coral $\delta^{18}O$ reflects both temperature and the $\delta^{18}O$ of seawater, with the latter being influenced by hydrological changes that could amplify or decrease the amplitude of the coral $\delta^{18}O$ seasonality. However, the rather smooth cycles of $\delta^{18}O$ and $\delta^{13}C$ values of our records showing little intra-annual noise bear no evidence that substantial changes in the stable isotope values of seawater have taken place over a year, and no similarity exists with the "irregular isotope pattern" characterizing intra-annual hydrological effects in sclerochronological datasets from many nearshore environments (Fig. 4, A and B) (*10*). The finding of maximum/minimum zooxanthellate photosynthesis having occurred during summer/winter, in phase with the annual irradiance cycle (*63*, *64*), further supports our notion of insignificant subannual variability of seawater isotope values, which we infer also from the fully marine, shallow-subtidal, and oligotrophic habitat housing an extremely diverse invertebrate fauna with more than 1000 mollusk species (*51*). We also note that the only slightly cuspate patterns of the $\delta^{13}C$ and $\delta^{18}O$ cycles in *Astreopora* reflect slowed, albeit continuous, growth during the cool season effected either by low winter SSTs or low winter irradiance or both. This is in accordance with the an-analogous situation of reef coral growth at a "high" latitude of ~45°N but in a context of low overall seasonality. A published gastropod sclerochronology (*Torquesia*) from PB that we ascribe to the MECO has provided an SST contrast of ~5°C [data from (*46*) using an SST slope for aragonite of −0.35‰ change in skeletal $\delta^{18}O$/°C) that is slightly below our finding from *Astreopora*. However, this record is rather short (n = 4 years), and the resolution of the time series is very heterogeneous between semiannual and almost monthly, which is why the reconstruction is likely to underestimate true seasonality.

Note, however, that looking at a very similar situation and latitude today and in the middle Eocene, a seasonal SST amplitude of 7° to 8°C is low for a high continentality of the shallow, inner PB gulf compared with ~10°C in the present-day open Atlantic off western France (44°N), or ~15°C in more continentally influenced sheltered bays of NW France (Fig. 1 and fig. S6). Similarly, the regional SST seasonality reported here was smaller than the seasonal air temperature changes on the neighboring European mainland (*34*, *36*). This suggests that SST seasonality of the gulf was likely amplified by mainland effects and, consequently, larger than SST seasonality in the adjacent open Atlantic. Our new datasets from PB show little evidence for biases by hydrologic changes beyond the temperature effect on $\delta^{18}O$ values. This distinguishes them significantly from most published data from the middle Lutetian of the PB-HB, which show the irregular isotope pattern (*44*, *46*, *47*, *49*). We relate this difference to the uplifting of the isthmus of Weald-Artois during the late Lutetian (Fig. 1) (*51*), which prevented any further influx of low-salinity waters from the Arctic/North Sea (*26*) into the PB-HB. The newly formed PB-HB gulf exclusively opened to the Atlantic and apparently remained fully marine (Fig. 1). For the MECO hyperthermal, this particular paleogeographic situation ensured $\delta^{18}O$ records dominated by the temperature effect. However, 7° to 8°C SST seasonality was otherwise more characteristic of paleolatitudes of ~27°N (U.S. Gulf Coast Region) in the middle Eocene before or after the MECO (*10*, *39*, *50*) and, in this respect, too low for a paleolatitude of ~45°N. Thus, in the wake of the MECO, both the long-term trend of Eocene global cooling and the long-term increase in temperature seasonality were temporarily halted. The lower seasonality during the MECO substantiates recent modeling results that Eocene seasonality was strongly coupled to atmospheric pCO_2 and sea level (*37*) and thus supports notions of a sea-level pulse during MECO (*27*).

Implications of the middle Eocene case study

Eocene, massive to pillow-shaped *Astreopora* from PB (Northwestern Europe) display extremely low rates of upward growth (0.2 to 0.3 cm year^{-1}), consistent with a paleogeographic position at the northern range limit of reef corals at that time. Here, we tested their potential as high-resolution environmental archive.

Annual density bands are consistent with stable isotope cycles ($\delta^{18}O$ and $\delta^{13}C$). No relationship exists between annual extension rate (0.2 to 1.4 cm year^{-1}) and annual mean stable isotope values ($\delta^{18}O$), i.e., no measurable extension rate–related kinetic isotope disequilibrium effect exists that discredits the use of slow-growing "tropical" reef corals as environmental archives. Mean skeletal $\delta^{18}O$ values may be used for reconstructions of seawater $\delta^{18}O$ values, i.e., the very negative mean $\delta^{18}O$ value of the two specimens is a reflection of a very negative $\delta^{18}O$ value of global seawater. According to the $\delta^{13}C$ values, we show that the Eocene *Astreopora* were zooxanthellate, and their calcification machinery is fully compatible with that of modern reef corals.

A pronounced relationship between extension rate and seasonal signal amplitude ($\delta^{18}O$) is not an artifact of differential sampling resolution. The seasonal range of $\delta^{18}O$ for an extension rate of 0.1 cm year^{-1} amounts 20% relative to seasonality at 1.4 cm year^{-1}. This amount of signal attenuation is largely equivalent with predictions by the sharp model of biosmoothing (*20*). However, seasonal signal attenuation only concerns the seasonal contrast of $\delta^{18}O$ values; the seasonal contrast of skeletal $\delta^{13}C$ is homogeneous at all extension rates studied. Thus, the observed patterns of signal attenuation is not very likely an effect of an extended skeletal residence time within calcifying tissue (=biosmoothing).

The calibration curve presented allows for correcting attenuations of measured signal amplitudes and the systematic use of *Astreopora* as environmental archive for the Eocene. The calibration procedure

described here to account for extension rate effects on stable isotope records may also turn out to be a powerful tool for using modern tropical reef corals with encrusting growth habits, e.g., from reef crests or level bottom communities, as climate archives.

Seasonal SST contrasts of the shallow PB were 7° to 8°C during the MECO (40 Ma ago), if $\delta^{18}O_{seawater}$ changes on seasonal time scales played a minor role for the coral $\delta^{18}O$ seasonality signal. Unlike previous sclerochronological studies on bivalves and gastropods, our new data have the advantage of providing consistent, inherently comparable temporal resolutions of individual years within the multi-year time series. According to the $\delta^{13}C$ values, maximum/minimum photosynthesis of the zooxanthellae occurred during summer/winter, in accord with a predominant forcing by seasonal irradiance changes. The annual amplitude of the $\delta^{13}C$ values is large compared with most published records of tropical and subtropical records and a likely expression of an enhanced, annual light-driven productivity contrast of photosynthesis by the symbionts at ~45°N.

Our findings clearly show that against all expectations (through problems related to sampling resolution, kinetic isotope disequilibria, and biosmoothing), massive and encrusting reef corals from marginal positions of the global coral reef belt have high potential as archives for proxy studies on past and current environmental change.

MATERIALS AND METHODS

The reef corals studied are housed at the geological and mineralogical collection of Leipzig University (Germany). The corals originally derive from Caumont/France (Sainte-Aulde) and were excavated from loose and partially cemented, highly fossiliferous sands, ascribed to the Sables d'Auvers, which are Bartonian in age (middle Eocene) (*46*, *54*). No further information regarding the site, facies, and stratigraphy is available from the museum labels. Today, the small pits no longer exist (coordinates: 48.994804°N, 3.201361°E), and the area is reforested. The Sables d'Auvers was assigned to the upper nannoplankton zone NP16 and can be ascribed to the MECO (*54*, *74*–*76*).

All corals (n = 38) represent abraded and rounded fragments of originally hemispherical and pillow-like growth forms (massive), showing internally rather flat to convex upward growth bands that curve downward near the margins of the colonies (fig. S1). Of these, two specimens of *Astreopora* were selected for this study (CAU-A3 and CAU-D4).

The *Astreopora* skeletons were cut with a rock saw at low tournament speed into slices along the plane of the corallites. The slices were ground to coplanar slabs of 6.0 ± 0.05–mm thickness, cleaned in an ultrasonic bath, and subsequently dried for 12 hours at 40°C. A thickness of 6.0 mm for the slabs is approximately equivalent with three layers of corallites and recommended for optimum contrasts and visibility of the annual density bands on x-ray images (*77*). Coral slabs were x-rayed with a digital x-ray cabinet (SHR 50 V), and digital x-ray photos were taken of the slabs used to visualize the density bands. For reconstructions of extension rate (centimeter $year^{-1}$), we followed the hypothesis that one couplet of bands of high and low density (high-density band and low-density band) is equivalent with 1 year of growth (*5*, *78*). Measurements of bulk density (gram $centimeter^{-3}$) were performed using x-ray densitometry from the same x-ray images using free CoralXDS software (*79*, *80*). Transects of density measurements were between 1.5 and 4.0 mm wide and aligned parallel with the corallites; measured bulk density therefore integrates over approximately three to six corallites and ensures to represent a representative mix of all skeletal elements, yet transects being narrow enough to avoid time-averaging effects from oblique geometries.

The coral slices were screened for diagenetic alteration according to the methods described in the literature (Supplementary Materials). In line with previous work (*55*), the corals studied were considered sufficiently well preserved for proxy analysis. Skeletal aragonite and microstructure are fully preserved, and intraskeletal porosity is unaffected by cementation (Supplementary Materials).

Consecutive samples for stable isotope analysis were taken from ledges following the trajectory of the corallites (3 × 3 mm in cross section). The ledges were cut out of the skeleton with a microdrill equipped with a thin stainless steel saw blade. Sampling increment widths were chosen according to the mean annual extension rate inferred from x-radiographs and selected to grant for ≥12 samples per year (better than monthly resolution). To avoid any sort of contamination, the ledges were cleaned in an ultrasonic bath and dried for 12 hours at 40°C. For the preparation of sample powders for stable isotope analysis, the ledges were fixed to a manually operated *XYZ* stage of a micromilling system and milled down at rectangular increments. Sampling increments for ledges #1 to #4 were 0.1 mm for specimen CAU-D4 and ledge #1 for CAU-A3, respectively (Fig. 2). To ensure plane milling surfaces and to avoid breakouts, the ledges were impregnated with dentist resin before milling (*23*). A positive side effect of impregnating the samples was that all skeletal pores were filled, and thus, there was no possibility of contamination by milling powders, which could be a severe problem especially with the low extension rates of the corals studied. For transects following corallites with high extension rate (>1 cm $year^{-1}$), samples for isotope analyses were drilled out of the slabs along a predefined path following single corallites (drill bit diameter of 0.6 mm and drilling depth of 1 mm) (Fig. 2). All of these procedures yielded ≥40 μg of sample powder per sample, which was the minimum amount of powder needed for a single analysis. Oxygen and carbon stable isotope ratios were measured at the Institute of Geophysics and Geology, Leipzig University (Germany). Carbonate powders were reacted with 105% phosphoric acid at 70°C using a Kiel IV online carbonate preparation line connected to a MAT 253 isotope ratio mass spectrometer. All carbonate values are reported in per mil (‰) relative to the VPDB standard. Reproducibility was monitored by replicate analysis of laboratory standards and was better than ±0.04‰ (1σ) for $\delta^{13}C$ and better than ±0.06‰ (1σ) for $\delta^{18}O$. The chemically inert resin has no measurable effect on the reproducibility of stable isotope analyses, even at very low carbonate/resin ratios (*23*). However, the amount of sample obtained from the small sample increments was insufficient for parallel analyses of stable isotopes and trace elements (e.g., Sr/Ca) as alternative proxies of SST. According to current knowledge, the use of resins also negatively affects chemical analyses, and no attempt was made, therefore, to produce combined stable isotope and trace element data.

The age models for each transect are based on the assumption that the most positive $\delta^{18}O$ values correspond to the coolest winter SSTs as anchor points for the age models, which is supported by the spatial coincidence of annual density banding pattern of high-density-band formation in winter and low-density-band formation during summer. The chronology for all points in between was derived by linear interpolation. For transects with small extension rates, the most negative $\delta^{13}C$ values were also used to define the winter (fig. S4). The mean of the seasonal range of the $\delta^{18}O$ and $\delta^{13}C$ values was calculated as the mean of the differences between

the most extreme summer value and the previous and subsequent winter maxima, and then averaged over all years.

To account for intra-annual isotope signal attenuation because of exceptionally low extension rates (biosmoothing), we extrapolated the sharp (Eq. 2) and "smooth" (Eq. 3) models of biosmoothing for modern *Porites* (*20*) to extension rates of <0.6 cm year^{-1}. For the extrapolation, we used the free software package PAST3 (*73*) and a nonlinear von Bertalanffy fit, which is a special form of a logistic function and commonly used in biological aging studies

Sharp model:

$$\text{Signal attenuation (\%)} = 99.088 * (1 - 0.95797 * \text{EXP}(-0.32426 * \text{extension rate [cm year}^{-1}])) \quad (2)$$

Smooth model:

$$\text{Signal attenuation (\%)} = 93.374 * (1 - 2.2107 * \text{EXP}(-0.20019 * \text{extension rate [mm year}^{-1}])) \quad (3)$$

In this study, we refer to biosmoothing in an entirely descriptive way for signal attenuations at small extension rates, because, naturally, no information exists on the original effective thickness of the tissue layer of the fossil corals.

SUPPLEMENTARY MATERIALS

Supplementary material for this article is available at https://science.org/doi/10.1126/sciadv.abm3875

REFERENCES AND NOTES

1. T. C. Brachert, M. Reuter, T. Felis, K. F. Kroeger, G. Lohmann, A. Micheels, C. Fassoulas, *Porites* corals from Crete (Greece) open a window into Late Miocene (10 Ma) seasonal and interannual climate variability. *Earth Planet. Sci. Lett.* **245**, 81–94 (2006).
2. T. Felis, Extending the instrumental record of ocean-atmosphere variability into the last interglacial using tropical corals. *Oceanography* **33**, 68–79 (2020).
3. R. C. Highsmith, Coral growth rates and environmental control of density banding. *J. Exp. Mar. Biol. Ecol.* **37**, 105–125 (1979).
4. J. M. Lough, Coral calcification from skeletal records revisited. *Mar. Ecol. Prog. Ser.* **373**, 257–264 (2008).
5. J. M. Lough, D. J. Barnes, Comparisons of skeletal density variations in *Porites* from the central Great Barrier Reef. *J. Exp. Mar. Biol. Ecol.* **155**, 1–25 (1992).
6. S. N. Burgess, M. T. McCulloch, G. E. Mortimer, T. M. Ward, Structure and growth rates of the high-latitude coral: *Plesiastrea versipora*. *Coral Reefs* **28**, 1005–1015 (2009).
7. J. A. Kleypas, J. W. McManus, L. A. B. Menez, Environmental limits to coral reef development. Where do we draw the line? *Am. Zool.* **39**, 146–159 (1999).
8. S. J. Fallon, M. T. McCulloch, R. van Woesik, D. J. Sinclair, Corals at their latitudinal limits: Laser ablation trace element systematics in *Porites* from Shirigai Bay, Japan. *Earth Planet. Sci. Lett.* **172**, 221–238 (1999).
9. R. B. Taylor, D. J. Barnes, J. M. Lough, Simple models of density band formation in massive corals. *J. Exp. Mar. Biol. Ecol.* **167**, 109–125 (1993).
10. T. Kobashi, E. L. Grossman, The oxygen isotopic record of seasonality in *Conus* shells and its application to understanding late Middle Eocene (38 Ma) climate. *Paleontol. Res.* **7**, 343–355 (2003).
11. S. Howe, A. Marshall, Temperature effects on calcification rate and skeletal deposition in the temperate coral, *Plesiastrea versipora* (Lamarck). *J. Exp. Mar. Biol. Ecol.* **275**, 63–81 (2002).
12. D. Thomson, D. Bearham, F. Graham, J. Eagle, High latitude, deeper water coral bleaching at Rottnest Island, Western Australia. *Coral Reefs* **30**, 1107 (2011).
13. D. A. Abdo, L. M. Bellchambers, S. N. Evans, Turning up the heat: Increasing temperature and coral bleaching at the high latitude coral reefs of the Houtman Abrolhos Islands. *PLOS ONE* **7**, e43878 (2012).
14. J. J. Leder, P. K. Swart, A. Szmant, R. E. Dodge, The origin of variations in the isotopic record of scleractinian corals: I. Oxygen. *Geochim. Cosmochim. Acta* **60**, 2857–2870 (1996).
15. J. N. Weber, P. M. J. Woodhead, Temperature dependence of oxygen-18 concentration in reef coral carbonates. *J. Geophys. Res.* **77**, 463–473 (1972).
16. T. Felis, J. Pätzold, Y. Loya, Mean oxygen-isotope signatures in *Porites* spp. corals: Inter-colony variability and correction for extension-rate effects. *Coral Reefs* **22**, 328–336 (2003).
17. T. McConnaughey, ^{13}C and ^{18}O isotopic disequilibrium in biological carbonates: I. Patterns. *Geochim. Cosmochim. Acta* **53**, 151–162 (1989).
18. T. Omata, A. Suzuki, T. Sato, K. Minoshima, E. Nomaru, A. Murakami, S. Murayama, H. Kawahata, T. Maruyama, Effect of photosynthetic light dosage on carbon isotope composition in the coral skeleton: Long-term culture of *Porites* spp. *J. Geophys. Res. Biogeosci.* **113**, G02014 (2008).
19. A. Suzuki, K. Hibino, A. Iwase, H. Kawahata, Intercolony variability of skeletal oxygen and carbon isotope signatures of cultured *Porites* corals: Temperature-controlled experiments. *Geochim. Cosmochim. Acta* **69**, 4453–4462 (2005).
20. M. K. Gagan, G. B. Dunbar, A. Suzuki, The effect of skeletal mass accumulation in *Porites* on coral Sr/Ca and δ^{18}O paleothermometry. *Paleoceanography* **27**, PA1203 (2012).
21. T. Felis, M. Ionita, N. Rimbu, G. Lohmann, M. Kölling, Mild and arid climate in the eastern Sahara-Arabian desert during the late Little Ice Age. *Geophys. Res. Lett.* **45**, 7112–7119 (2018).
22. J. Sadler, G. E. Webb, L. D. Nothdurft, B. Dechnik, Geochemistry-based coral palaeoclimate studies and the potential of "non-traditional" (non-massive *Porites*) corals: Recent developments and future progression. *Earth Sci. Rev.* **139**, 291–316 (2014).
23. P. Spreter, R. Reuter, T. C. Brachert, D. K. Kersting, Ultra-high-resolution stable isotope sampling of slow-growing and fragile coral skeletons. *Palaeogeogr. Palaeoclimatol. Palaeoecol.* **560**, 109992 (2020).
24. T. Westerhold, N. Marwan, A. J. Drury, D. Liebrand, C. Agnini, E. Anagnostou, J. S. K. Barnet, S. M. Bohaty, D. de Vleeschouwer, F. Florindo, T. Frederichs, D. A. Hodell, A. E. Holbourn, D. Kroon, V. Lauretano, K. Littler, L. J. Lourens, M. Lyle, H. Pälike, U. Röhl, J. Tian, R. H. Wilkens, P. A. Wilson, J. C. Zachos, An astronomically dated record of Earth's climate and its predictability over the last 66 million years. *Science* **369**, 1383–1387 (2020).
25. D. Evans, N. Sagoo, W. Renema, L. J. Cotton, W. Müller, J. A. Todd, P. K. Saraswati, P. Stassen, M. Ziegler, P. N. Pearson, P. J. Valdes, H. P. Affek, Eocene greenhouse climate revealed by coupled clumped isotope-Mg/Ca thermometry. *Proc. Natl. Acad. Sci.* **115**, 1174–1179 (2018).
26. M. Baatsen, A. S. von der Heydt, M. Huber, M. A. Kliphuis, P. K. Bijl, A. Sluijs, H. A. Dijkstra, The Middle to Late Eocene greenhouse climate modelled using the CESM 1.0.5. *Clim. Past* **16**, 2573–2597 (2020).
27. M. J. Henehan, K. M. Edgar, G. L. Foster, D. E. Penman, P. M. Hull, R. Greenop, E. Anagnostou, P. N. Pearson, Revisiting the Middle Eocene Climatic Optimum "carbon cycle conundrum" with new estimates of atmospheric pCO2 from boron isotopes. *Paleoceanogr. Paleoclimatol.* **35**, e2019PA003713 (2020).
28. M. J. Cramwinckel, H. K. Coxall, K. K. Śliwińska, M. Polling, D. T. Harper, P. K. Bijl, H. Brinkhuis, J. S. Eldrett, A. J. P. Houben, F. Peterse, S. Schouten, G.-J. Reichart, J. C. Zachos, A. Sluijs, A warm, stratified, and restricted Labrador Sea across the Middle Eocene and its climatic optimum. *Paleoceanogr. Paleoclimatol.* **35**, e2020PA003932 (2020).
29. A. van der Boon, K. F. Kuiper, R. van der Ploeg, M. J. Cramwinckel, M. Honarmand, A. Sluijs, W. Krijgsman, Exploring a link between the Middle Eocene Climatic Optimum and Neotethys continental arc flare-up. *Clim. Past* **17**, 229–239 (2021).
30. R. van der Ploeg, D. Selby, M. J. Cramwinckel, Y. Li, S. M. Bohaty, J. J. Middelburg, A. Sluijs, Middle Eocene greenhouse warming facilitated by diminished weathering feedback. *Nat. Commun.* **9**, 2877 (2018).
31. E. Anagnostou, E. H. John, T. L. Babila, P. F. Sexton, A. Ridgwell, D. J. Lunt, P. N. Pearson, T. B. Chalk, R. D. Pancost, G. L. Foster, Proxy evidence for state-dependence of climate sensitivity in the Eocene greenhouse. *Nat. Commun.* **11**, 4436 (2020).
32. M. J. Cramwinckel, M. Huber, I. J. Kocken, C. Agnini, P. K. Bijl, S. M. Bohaty, J. Frieling, A. Goldner, F. J. Hilgen, E. L. Kip, F. Peterse, R. van der Ploeg, U. Röhl, S. Schouten, A. Sluijs, Synchronous tropical and polar temperature evolution in the Eocene. *Nature* **559**, 382–386 (2018).
33. J. S. Eldrett, D. R. Greenwood, I. C. Harding, M. Huber, Increased seasonality through the Eocene to Oligocene transition in northern high latitudes. *Nature* **459**, 969–973 (2009).
34. V. Mosbrugger, T. Utescher, D. L. Dilcher, Cenozoic continental climatic evolution of Central Europe. *Proc. Natl. Acad. Sci. U.S.A.* **102**, 14964–14969 (2005).
35. M. Huber, R. Caballero, The Early Eocene equable climate problem revisited. *Clim. Past* **7**, 603–633 (2011).
36. T. Utescher, O. V. Bondarenko, V. Mosbrugger, The Cenozoic cooling–Continental signals from the Atlantic and Pacific side of Eurasia. *Earth Planet. Sci. Lett.* **415**, 121–133 (2015).
37. A. Toumoulin, D. Tardif, Y. Donnadieu, A. Licht, J. B. Ladant, L. Kunzmann, G. Dupont-Nivet, Evolution of continental temperature seasonality from the Eocene greenhouse to the Oligocene icehouse–A model-data comparison. *Clim. Past* **18**, 341–362 (2022).
38. T. Utescher, A. A. Bruch, B. Erdei, L. François, D. Ivanov, F. M. B. Jacques, A. K. Kern, Y. S.(C.). Liu, V. Mosbrugger, R. A. Spicer, The coexistence approach—Theoretical background and

practical considerations of using plant fossils for climate quantification. *Palaeogeogr. Palaeoclimatol. Palaeoecol.* **410**, 58–73 (2014).
39. L. C. Ivany, K. C. Lohmann, W. P. Patterson, in *From Greenhouse to Icehouse: The marine Eocene-Oligocene transition*, D. R. Prothero, Ivany, L.C., Elizabeth A. Nesbitt, Eds. (Columbia Univ. Press, 2003), pp. 232–251.
40. T. Kobashi, E. L. Grossman, T. E. Yancey, D. T. Dockery III, Reevaluation of conflicting Eocene tropical temperature estimates: Molluskan oxygen isotope evidence for warm low latitudes. *Geology* **29**, 983–986 (2001).
41. L. Bougeois, M. de Rafélis, G. J. Reichart, L. J. de Nooijer, F. Nicollin, G. Dupont-Nivet, A high resolution study of trace elements and stable isotopes in oyster shells to estimate Central Asian Middle Eocene seasonality. *Chem. Geol.* **363**, 200–212 (2014).
42. F. P. Andreasson, B. Schmitz, Temperature seasonality in the early Middle Eocene North Atlantic region: Evidence from stable isotope profiles of marine gastropod shells. *Geol. Soc. Am. Bull.* **112**, 628–640 (2000).
43. A. Tripati, J. C. Zachos, Paleocene and Eocene coastal ocean temperatures. *GFF* **122**, 171–172 (2000).
44. F. P. Andreasson, B. Schmitz, Winter and summer temperatures of the early middle Eocene of France from *Turritella* δ18O profiles. *Geology* **24**, 1067–1070 (1996).
45. F. P. Andreasson, B. Schmitz, Tropical Atlantic seasonal dynamics in the early Middle Eocene from stable oxygen and carbon isotope profiles of mollusk shells. *Paleoceanography* **13**, 183–192 (1998).
46. D. Huyghe, F. Lartaud, L. Emmanuel, D. Merle, M. Renard, Paleogene climate evolution in the Paris Basin from oxygen stable isotope ($\delta^{18}O$) compositions of marine molluscs. *J. Geol. Soc. Lond.* **142**, 1–12 (2015).
47. D. Huyghe, D. Merle, F. Lartaud, E. Cheype, L. Emmanuel, Middle Lutetian climate in the Paris Basin: Implications for a marine hotspot of paleobiodiversity. *Facies* **58**, 587–604 (2012).
48. L. Purton, M. Brasier, Gastropod carbonate $\delta^{18}O$ and $\delta^{13}C$ values record strong seasonal productivity and stratification shifts during the Late Eocene in England. *Geology* **25**, 871–874 (1997).
49. N. J. de Winter, J. Vellekoop, A. J. Clark, P. Stassen, R. P. Speijer, P. Claeys, The giant marine gastropod *Campanile giganteum* (Lamarck, 1804) as a high-resolution archive of seasonality in the Eocene greenhouse world. *Geochem. Geophys. Geosyst.* **21**, e2019GC008794 (2020).
50. D. J. J. van Hinsbergen, L. V. de Groot, S. J. van Schaik, W. Spakman, P. K. Bijl, A. Sluijs, C. G. Langereis, H. Brinkhuis, A paleolatitude calculator for paleoclimate studies (model version 2.1). *PLOS ONE* **10**, e0126946 (2015).
51. D. Merle, *Stratotype Lutétien* (BRGM, 2008), pp. 288.
52. S. Dominici, S. Zuschin, Palaeocommunities, diversity and sea-level change from Middle Eocene shell beds of the Paris Basin. *J. Geol. Soc. Lond.* **173**, 889–900 (2016).
53. J.-C. Gall, *Sedimentationsräume und Lebensbereiche der Erdgeschichte-eine Einführung in die Paläoökologie* (Springer-Verlag, 1983).
54. J.-P. Gély, Le Paléogène du Bassin du Paris: Corrélation et reconstitutions paléogéographiques. *Bull. Inf. Géol. Bassin Paris* **53**, 2–13 (2016).
55. C. H. White, dissertation, University of London (2013).
56. C. Perrin, W. Kiessling, Latitudinal trends in Cenozoic reef patterns and their relationsship to climate. *Int. Assoc. Sedimentol. Spec. Publ.* **42**, 17–34 (2010).
57. C. C. Wallace, B. R. Rosen, Diverse staghorn corals (*Acropora*) in high-latitude Eocene assemblages: Implications for the evolution of modern diversity patterns of reef corals. *Proc. Biol. Sci.* **273**, 975–982 (2006).
58. T. M. DeCarlo, A. L. Cohen, Dissepiments, density bands and signatures of thermal stress in *Porites* skeletons. *Coral Reefs* **36**, 749–761 (2017).
59. J. Carilli, R. Norris, B. Black, S. Walsh, M. McField, Local stressors reduce coral resilience to bleaching. *PLOS ONE* **4**, e6324 (2009).
60. J. H. Hudson, E. A. Shinn, R. B. Halley, B. H. Lidz, Sclerochronology: A tool for interpreting past environments. *Geology* **4**, 361–364 (1976).
61. A. G. Grottoli, C. M. Eakin, A review of modern coral $\delta^{18}O$ and $\Delta^{14}C$ proxy records. *Earth Sci. Rev.* **81**, 67–91 (2007).
62. K. Frankowiak, X. T. Wang, D. M. Sigman, A. M. Gothmann, M. V. Kitahara, M. Mazur, A. Meibom, J. Stolarski, Photosymbiosis and the expansion of shallow-water corals. *Sci. Adv.* **2**, e1601122 (2016).
63. P. K. Swart, Carbon and oxygen isotope fractionation in scleractinian corals: A review. *Earth Sci. Rev.* **19**, 51–80 (1983).
64. P. K. Swart, J. J. Leder, A. M. Szmant, R. E. Dodge, The origin of variations in the isotopic record of scleractinian corals: II. Carbon. *Geochim. Cosmochim. Acta* **60**, 2871–2885 (1996).
65. C. Maier, T. Felis, J. Pätzold, R. P. M. Bak, Effect of skeletal growth and lack of species effects in the skeletal oxygen isotope climate signal within the coral genus *Porites*. *Mar. Geol.* **207**, 193–208 (2004).
66. J. Uchikawa, R. E. Zeebe, The effect of carbonic anhydrase on the kinetics and equilibrium of the oxygen isotope exchange in the CO_2-H_2O system: Implications for $\delta^{18}O$ vital effects in biogenic carbonates. *Geochim. Cosmochim. Acta* **95**, 15–34 (2012).
67. S. Hirabayashi, Y. Yokoyama, A. Suzuki, Y. Kawakubo, Y. Miyairi, T. Okai, S. Nojima, Coral growth-rate insensitive Sr/Ca as a robust temperature recorder at the extreme latitudinal limits of *Porites*. *Geochem. J.* **47**, e1–e5 (2013).
68. M. Inoue, A. Suzuki, M. Nohara, K. Hibino, H. Kawahata, Empirical assessment of coral Sr/Ca and Mg/Ca ratios as climate proxies using colonies grown at different temperatures. *Geophys. Res. Lett.* **34**, L12611 (2007).
69. E. C. Hathorne, T. Felis, A. Suzuki, H. Kawahata, G. Cabioch, Lithium in the aragonite skeletons of massive *Porites* corals: A new tool to reconstruct tropical sea surface temperatures. *Paleoceanography* **28**, 143–152 (2013).
70. N. F. Goodkin, K. Hughen, A. C. Cohen, S. R. Smith, Record of Little Ice Age sea surface temperatures at Bermuda using a growth-dependent calibration of coral Sr/Ca. *Paleoceanography* **20**, PA4016 (2005).
71. J. A. Crame, Early Cenozoic evolution of the latitudinal diversity gradient. *Earth Sci. Rev.* **202**, 103090 (2020).
72. P. K. Swart, The geochemistry of carbonate diagenesis: The past, present and future. *Sedimentology* **62**, 1233–1304 (2015).
73. Ø. Hammer, D. A. T. Harper, P. D. Ryan, PAST: Paleontological statistics software package for education and data analysis. *Palaeontol. Electron.* **4**, 1–9 (2001).
74. M. Giorgioni, L. Jovane, E. S. Rego, D. Rodelli, F. Frontalini, R. Coccioni, R. Catanzariti, E. Özcan, Carbon cycle instability and orbital forcing during the Middle Eocene Climatic Optimum. *Sci. Rep.* **9**, 9357 (2019).
75. M.-P. Aubry, Paleogene calcareous nannoplankton biostratigraphy of northwestern Europe. *Palaeogeogr. Palaeoclimatol. Palaeoecol.* **55**, 267–334 (1986).
76. F. M. Gradstein, J. Ogg, M. Schmitz, G. Ogg, *The Geologic Timescale 2012* (Elsevier, 2012), vol. 1.
77. M. D. A. A. Le Tissier, B. Clayton, B. E. Brown, P. Spencer Davis, Skeletal correlates of coral density banding and an evaluation of radiography as used in sclerochronology. *Mar. Ecol. Prog. Ser.* **110**, 29–44 (1994).
78. J. H. Hudson, Growth rates of *Montastrea cavernosa*—A record of environmental change in Key Largo Coral Reef Marine Sanctuary. *Bull. Mar. Sci.* **31**, 444–459 (1981).
79. K. P. Helmle, K. E. Kohler, R. E. Dodge, Proceedings 9th International Coral Reef Symposium, (Nova Southeastern University, Fort-Lauderdale-Davie, 2002), Bali, Indonesia, 23 to 27 October 2000, Vol. 1, pp. 365-371.
80. K. P. Helmle, R. E. Dodge, P. K. Swart, D. K. Gledhill, C. M. Eakin, Growth rates of Florida corals from 1937 to 1996 and their response to climate change. *Nat. Commun.* **2**, 6 (2011).
81. A. M. Gothmann, J. Stolarski, J. F. Adkins, B. Schoene, K. J. Dennis, D. P. Schrag, M. Mazur, M. L. Bender, Fossil corals as an archive of secular variations in seawater chemistry since the Mesozoic. *Geochim. Cosmochim. Acta* **160**, 188–208 (2015).
82. T. C. Brachert, T. Corrège, M. Reuter, C. Wrozyna, L. Londeix, P. Spreter, C. Perrin, An assessment of reef coral calcification over the late Cenozoic. *Earth Sci. Rev.* **204**, 103154 (2020).
83. L. Milliere, O. Hasinger, S. Bindschedler, G. Cailleau, J. E. Spangenberg, E. P. Verrecchia, Stable carbon and oxygen isotope signatures of pedogenic needle fibre calcite. *Geoderma* **161**, 74–87 (2011).
84. J. Stolarski, Three-dimensional micro- and nanostructural characteristics of the scleractinian coral skeleton: A biocalcification proxy. *Acta Palaeontol. Pol.* **48**, 497–530 (2003).
85. P. Forjanes, M. S. Roda, M. Greiner, E. Griesshaber, N. A. Lagos, S. Veintemillas-Verdaguer, J. M. Astilleros, L. Fernández-Díaz, W. W. Schmahl, Long-term experimental diagenesis of aragonitic biocarbonates: From organic matter loss to abiogenic calcite formation. *Biogeosciences Discuss.* **2021**, 1–53 (2021).
86. S. R. Dickinson, K. M. McGrath, Quantitative determination of binary and tertiary calcium carbonate mixtures using powder x-ray diffraction. *Analyst* **126**, 1118–1121 (2001).
87. F. Lartaud, L. Emmanuel, M. de Rafelis, M. Ropert, N. Labourdette, C. A. Richardson, M. Renard, A latitudinal gradient of seasonal temperature variation recorded in oyster shells from the coastal waters of France and The Netherlands. *Facies* **56**, 13–25 (2010).

Acknowledgments: Two reviewers made helpful suggestions on how to improve our manuscript. M. Siron from Val-d'Oise Natural Reserve (France) is thanked for excellent support of our fieldwork. S. Wurlitzer (Leipzig) provided microscopic photographs. S. Ćorić (Vienna, Austria) determined coccoliths entrapped within the coral skeletons. **Funding:** Funding by the Deutsche Forschungsgemeinschaft (AOBJ641985) is acknowledged. We acknowledge support from Leipzig University for Open Access Publishing. **Author contributions:** Conceptualization: T.C.B. Methodology: T.C.B., P.M.S., and M.H. Investigation: T.C.B., M.R., M.H., and P.M.S. Supervision: T.C.B. Writing (original draft): T.C.B., C.G., and T.F. **Competing interests:** The authors declare that they have no competing interests. **Data and materials availability:** All data needed to evaluate the conclusions in the paper are present in the paper and/or the Supplementary Materials.

Submitted 14 September 2021
Accepted 7 April 2022
Published 20 May 2022
10.1126/sciadv.abm3875

Slow-growing reef corals as climate archives: A case study of the Middle Eocene Climatic Optimum 40 Ma ago

Thomas C. BrachertThomas FelisCyril GagnaisonMarlene HoehleMarkus ReuterPhilipp M. Spreter

Sci. Adv., 8 (20), eabm3875. • DOI: 10.1126/sciadv.abm3875